ADVANCED OPTICAL MATERIALS
www.advopticalmat.de

Performance Boost by Dark Electro Treatment in MACl-Added $FAPbI_3$ Perovskite Solar Cells

*Mikhail Pylnev, Ryosuke Nishikubo, Fumitaka Ishiwari, Atsushi Wakamiya, and Akinori Saeki**

Halide anion migration in organic–inorganic metal halide perovskites significantly influences the power conversion efficiency (PCE) and hysteresis of perovskite solar cells (PSCs). These materials are sensitive to various external stimuli such as light, heat, and electrical bias, highlighting the need for novel post-manufacturing treatment methods alongside a deeper understanding of their mechanisms. Here, a dark electro (DE) treatment is introduced that applies a negative-positive-negative bias to PSC under dark conditions, which is particularly effective for formamidinium (FA) lead iodide ($FAPbI_3$) PSCs processed with a methylammonium chloride (MACl) additive. The DE treatment, followed by light soaking, results in an average PCE increase of 2.9 ± 1.8% (from an initial 18.2 ± 2.0% to 21.1 ± 0.8% after treatment) with a notable decrease in deviation. It is discovered that residual chloride anions from MACl play a critical role in the DE treatment. The migration of halide anions under a shaking electric bias is investigated using energy-dispersive X-ray spectroscopy (EDX) and time-of-flight secondary ion mass spectroscopy (TOF-SIMS). This study elucidates the distribution and impact of residual chloride anions, providing insights into the mechanisms underlying the DE treatment.

1. Introduction

Metal halide perovskites, a novel class of semiconductors characterized by soft and reconfigurable ionic bonds, offer great potential for various applications because of their unique and adjustable physical properties. Over the past decade, significant progress has been made in the development of perovskite solar cells (PSCs), with the power conversion efficiency (PCE) increasing impressively from 3.8% to 26.1%.[1–4] Nevertheless, the intrinsic instability under light, heat, electrical bias, and ion migration within these devices remains a critical challenge. Numerous studies have identified ion instabilities and trapped charges as primary factors contributing to this instability. While some reports have highlighted the beneficial effects of ion migration, such as defect healing,[5,6] most studies have indicated that halide migration and segregation lead to instabilities.[7–10] Ion migration is induced by an external electric field,[11–13] causing hysteresis under forward and reverse voltage.[9,14–16] Despite extensive research, questions remain regarding the primary routes of migration and their underlying mechanisms.[17]

Given the reconfigurable ionic bonding of the perovskites and the delicate organic charge transport layer (e.g., spiro-OMeTAD), post-manufacturing treatments are effective in enhancing the initial PCE of as-prepared devices. As illustrated in **Figure 1a**, conventional non-electric post-treatments such as light soaking under pseudo-sunlight and dark storage facilitate trap-filling, ion migration, and chemical doping of spiro-OMeTAD.[18] Additionally, Huang et al. introduced a reverse-biased electric treatment to increase the efficiency of PSCs (Figure 1b).[19] They attributed the observed efficiency gain to ion migration and their interactions with the SnO_2 electron transport layer (ETL), leading to an increased open-circuit voltage (V_{OC}). Jeong et al. described a novel "pulsatile therapy", which applies short electrical pulses of reverse bias.[20] This treatment was also attributed to the

M. Pylnev, R. Nishikubo, F. Ishiwari, A. Saeki
Department of Applied Chemistry
Graduate School of Engineering
Osaka University
2-1 Yamadaoka, Suita, Osaka 565–0871, Japan
E-mail: saeki@chem.eng.osaka-u.ac.jp

The ORCID identification number(s) for the author(s) of this article can be found under https://doi.org/10.1002/adom.202401902

DOI: 10.1002/adom.202401902

R. Nishikubo, F. Ishiwari, A. Saeki
Innovative Catalysis Science Division
Institute for Open and Transdisciplinary Research Initiatives (ICS-OTRI)
Osaka University
1-1 Yamadaoka, Suita, Osaka 565–0871, Japan

F. Ishiwari
PRESTO
Japan Science and Technology Agency (JST)
Kawaguchi, Saitama 332-0012, Japan

A. Wakamiya
Institute for Chemical Research
Kyoto University
Uji, Kyoto 611-0011, Japan

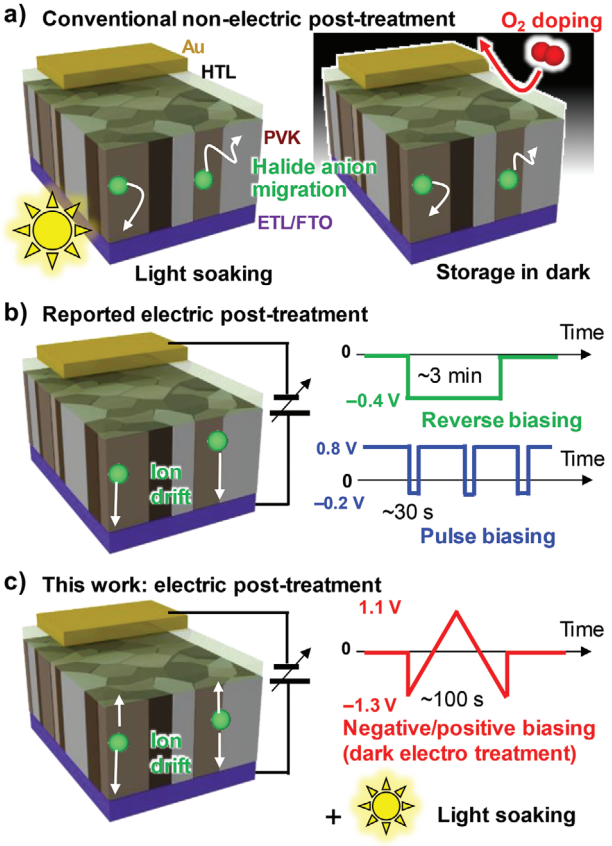

Figure 1. Illustration of post-manufacturing treatment. a) Conventional non-electric treatments of (left panel) light soaking and (right panel) storage in darkness, including O_2 doping. The halide anion migration is represented by green spheres. b) Reported electric post-treatment of reverse biasing[19] and pulse biasing.[20] c) Electric post-treatment in this work (DE treatment followed by light soaking).

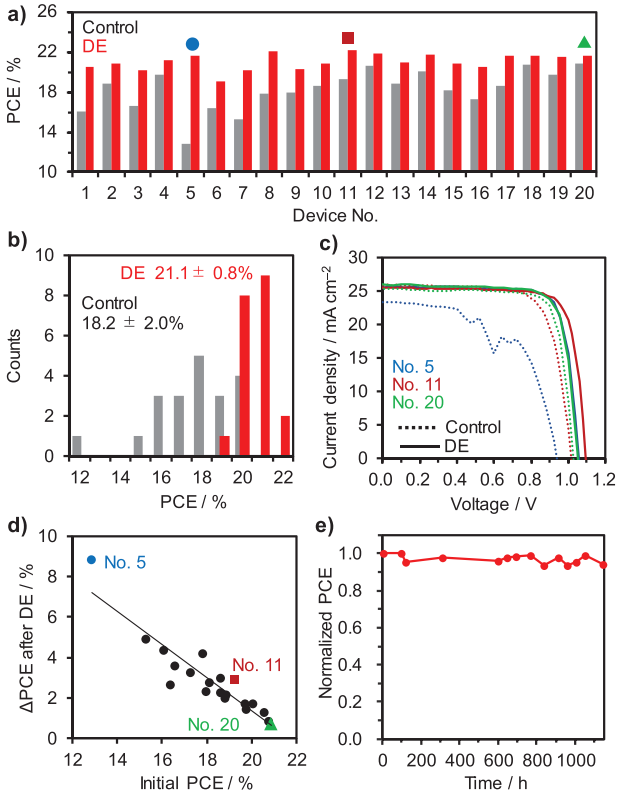

Figure 2. a) PCE values of twenty individual $FAPbI_3$ PSCs processed with MACl. Gray represents the control and red represents DE treatment. b) Statistics of PCEs: the values of average and standard deviation are appended. c) *JV* curves of devices No. 5, 11, and 20. These correspond to the circle, square, and triangle symbols in (a). Dotted lines represent before DE treatment and solid lines represent after DE treatment. The curves were obtained under the reverse scan. d) Plot of ΔPCE versus initial PCE before DE treatment. e) Stability of the DE-treated device (the initial PCE: 20.06%) stored in a sealed box outside a glovebox at 20–25 °C and 30–60% RH.

redistribution of iodine ions, leading to the return of halide defects to shallow-level states. In these studies,[19,20] methylammonium chloride (MACl) was added to precursor solutions of $FAPbI_3$ and $MAPbI_3$ perovskites (FA: formamidinium) to improve their morphology, grain size, and crystallinity.[21–24] The rapid initial formation of the perovskite structure in the presence of MACl is attributed to the higher diffusivity of Cl^- ions compared to I^- ions.[25]

Considering the evaporation point of MACl (175–225 °C)[26] and the typical thermal annealing temperature of $FAPbI_3$ (150 °C),[27] residual Cl^- possibly exists in the films. Takahashi et al. identified Cl traces in $FAPbI_3$ prepared with MACl using inductively coupled plasma mass spectrometry.[28] Yuan et al. found that after treatment with cyclohexylmethylammonium iodide, the chlorine/iodine ratio on the perovskite surface increased from 0.037 to 0.439, enhancing photovoltaic performance.[29] Indeed, the activation energy of Cl^- diffusion (0.2 eV)[30] is three times smaller than that of I^- (0.6 eV).[31] However, the influence of residual Cl^- has been overlooked, thus missing an opportunity to fully understand and optimize the material properties.

In this study, we introduce a novel post-manufacturing approach called dark electro (DE) treatment. As illustrated in Figure 1c, a negative (−1.3 V)-positive (1.1 V)-negative (−1.3 V) bias is applied to a PSC within ≈100 s (0.02 V step with 1 s hold time for each) under dark conditions. Note that this ≈2 min reverse/forward DE treatment can be repeated to achieve a higher PCE under pseudo-sunlight. This method leverages the unique properties of halide migration to enhance the performance of $FAPbI_3$-based PSC processed with MACl (33 mol% in this study). We reveal a beneficial redistribution of ionic species, particularly residual Cl^- within the perovskite layer, using scanning electron microscopy and energy- dispersive X-ray spectroscopy (SEM-EDX) and time-of-flight secondary ion mass spectroscopy (TOF-SIMS). DE treatment not only enhances the PCE but also improves the reproducibility of PSCs. Our work offers deeper insights into the influence of ionic movement on the overall performance of $FAPbI_3$-based PSCs.

2. Results and Discussion

Figure 2a shows the PCE values of $FAPbI_3$ with MACl PSCs before and after the DE treatment of 20 individual devices (detailed data are provided in Figure S1 and Table S1, Supporting

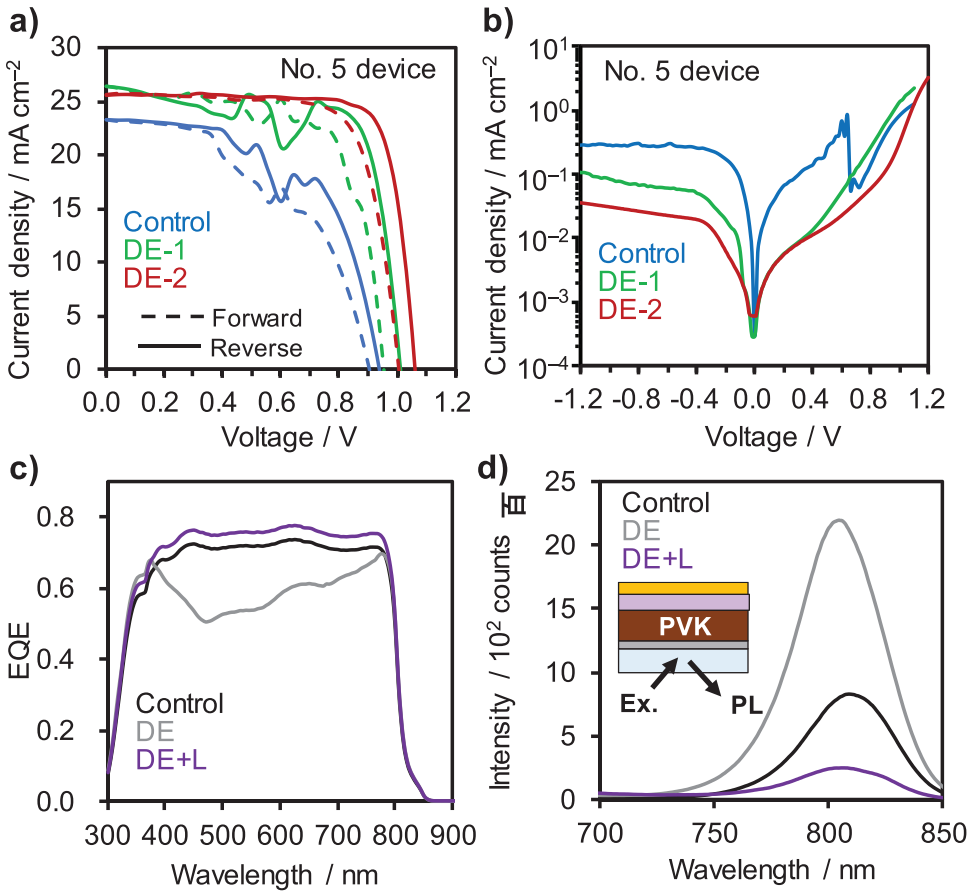

Figure 3. Transient change of a) *JV* curves under illumination and b) dark *JV* curves of device No. 5 (see Figure 2, MACl-added $FAPbI_3$). The blue, green, and red curves are the control, DE-1 (after one DE treatment), and DE-2 (after four DE treatments), respectively. The dashed and solid lines in (a) represent the forward and reverse scans, respectively. c) EQE spectra and d) PL spectra of an MACl-added $FAPbI_3$ device before DE (black), immediately after DE (DE, gray), and after light soaking (DE + L, purple). The inset in (d) shows the geometry of the PL measurement, where Ex is the excitation light and PVK is the perovskite.

Information). The DE treatment successfully improved the PCE from 18.2 ± 2.0% to 21.1 ± 0.8%, as shown in the statistics (Figure 2b). The average increase in PCE (ΔPCE) is 2.9 ± 1.8%, which is comparable to a typical passivation effect of PSCs.[32–34] The current density (*J*)-voltage (*V*) curves before and after DE are shown in Figure 2c for the devices that exhibited the largest ΔPCE (No. 5 in Figure 2a), the highest PCE after DE treatment (No. 11), and the highest PCE before DE treatment (No. 20). Device No. 5 achieved a significant gain in PCE from 12.9% to 21.7% with DE treatment. This prominent gain is attributed to increases in V_{OC} (0.937–1.059 V by 0.122 V) and fill factor (FF, 0.588–0.799 by 0.211). The average gains for each device parameter over 20 devices were 3.5% for the short-circuit current density (J_{SC}), 5.0% for V_{OC}, and 6.9% for FF (Figure S2, Supporting Information). Notably, ΔPCE is inversely correlated with the initial PCE before DE treatment (Figure 2d), indicating that initially low-performing devices can achieve significant gains and reach high PCE levels. The lasting improvement in PCE after DE treatment is also noteworthy (≈120 s shown in Figure S3, Supporting Information). In addition to this short-term stability, the normalized PCE was maintained at more than 90% after 1000 h of storage at 20–25 °C and 30–60% relative humidity (RH) (Figure 2f). The external quantum efficiency (EQE) spectrum showed a flat shape with the integrated J_{SC} value of 23.87 mA cm^{-2} (Figure S4, Supporting Information).

Given that the post-treatment included a few cycles of DE treatment and light soaking, we analyzed the transient changes in the *JV* curves and photophysical characteristics in detail. **Figure 3a** shows the *JV* curves of device No. 5 (with the largest ΔPCE) before (control) and after applying one or four DE treatments (DE-1 and DE-2, respectively). The PCE increased continuously from 12.9% for the control to 19.8% for DE-1 and 21.7%for DE-2 (Table S2, Supporting Information). The first two *JV* curves were unstable, likely due to disturbances in the ionic system, which is known to participate in current movements in PSCs.[35] Figure 3b shows the corresponding dark *JV* curves obtained during the DE treatment. The dark current in the negative bias region decreased from ≈0.3 to 0.1 mA cm^{-2} after the first DE treatment (DE-1) and further decreased to ≈0.03 mA cm^{-2} after four DE treatments (DE-2). This improvement aligns with the enhanced photovoltaic performance observed after DE treatment. Along with a threefold increase in R_{sh}, the series resistance (R_s) decreased twofold, significantly improving the PCE. The hysteresis index also dropped from 0.20 to 0.12 after the DE treatments, indicating a stabilized

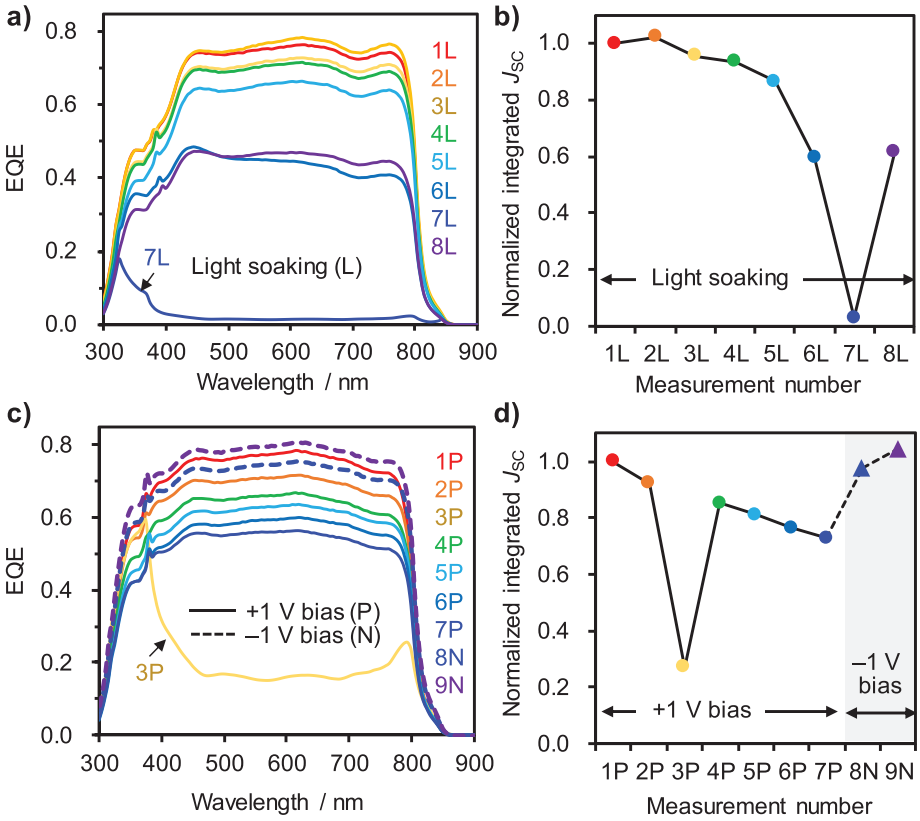

Figure 4. a) EQE spectra after light soaking (L) for 2 min (1–8L represent the sequential measurements). b) Normalized J_{SC}^{EQE} of (a) with the sequential measurement number. c) EQE spectra after applying positive (+1 V, 1P–7P, solid line) and negative (−1 V, 8N–9N, dashed line) bias in darkness. 1P–9N represent the sequential measurements. d) Normalized J_{SC}^{EQE} of (c) with the sequential measurement number. Note that the EQE spectra were measured at 0 V bias (short circuit) upon exposure to a scanned monochromated light. 7L in (a) and 3P in (c) that show an exceptional shape are indicated with arrows (see main text).

ionic system related to ion migration and accumulation at the interfaces.[36] The increase in charge carrier lifetimes (control: 148 µs and DE: 208 µs in Figure S5 and Table S3, Supporting Information) observed in transient photovoltage (TPV) measurements supports the reduction of charge traps by DE treatment.

Figure 3c shows the EQE spectra of the MACl-added $FAPbI_3$ PSC before and after DE treatment. The EQE spectrum before DE was flat; however, after DE, it was suppressed and irregularly deformed in the 400–800 nm region. Notably, the EQE increased after light irradiation (DE + L). This distinct change in the EQE aligns with the photoluminescence (PL) spectra (Figure 3d), where electron extraction is degraded after DE (increased PL) and subsequently improved by light soaking (decreased PL). The decrease in electron extraction immediately after DE may be explained by the deactivation of perovskite grains.[9] Namely, ions and vacancies gather at the ETL and hole transporting layer (HTL) interfaces, becoming recombination centers and increasing contact resistance. Light soaking helps ions to rearrange and redistribute homogenously in ionic systems.[37]

To clarify the observed irregular changes in EQE, we performed repeated EQE measurements after exposure to pseudo-sunlight (1 sun for 2 min) (**Figure 4a**). As summarized in Figure 4b, the normalized J_{SC} integrated over the EQE spectrum (J_{SC}^{EQE}) increased marginally during the second cycle of light irradiation (2L), in accordance with the literature.[37–39] This increase likely stemmed from the light-induced doping of spiro-OMeTAD[39] and/or the rearrangement of loosely bound ions.[37] However, the J_{SC}^{EQE} values continuously decreased from the third to the seventh cycles (3L–7L). In particular, the EQE spectrum at 7L exhibited almost canceling features from 400 to 800 nm, similar to the observations shown in Figure 3c. This phenomenon will be discussed further in the next paragraph. Figure 4c shows the EQE spectra at positive (+1 V, 1P–7P) and negative (−1 V, 8N–9N) biases in darkness. The normalized J_{SC}^{EQE} values in Figure 4d exhibit a steep decrease at a positive bias (1P–7P). This was explained by the migration of I^- to the HTL and the consequent accumulation of I vacancies at the ETL.[40] Notably, a rapid drop at 3P and recovery at 4P were observed during positive biasing, similar to the phenomenon observed under light soaking (7L in Figure 4b), Applying a negative bias restored and improved the initial EQE spectra (8 and 9N).

A sudden drop in EQE signal was observed for samples under positive bias (3P in Figure 4c), light soaking (7L in Figure 4a), and DE treatment (DE in Figure 3c). The suppression of the EQE signal at most wavelengths (400–800 nm) could be attributed to the deactivation of perovskite grains caused by ionic migration.[9,41] However, the EQE signal was still observed at wavelengths below ≈450 nm. Under light

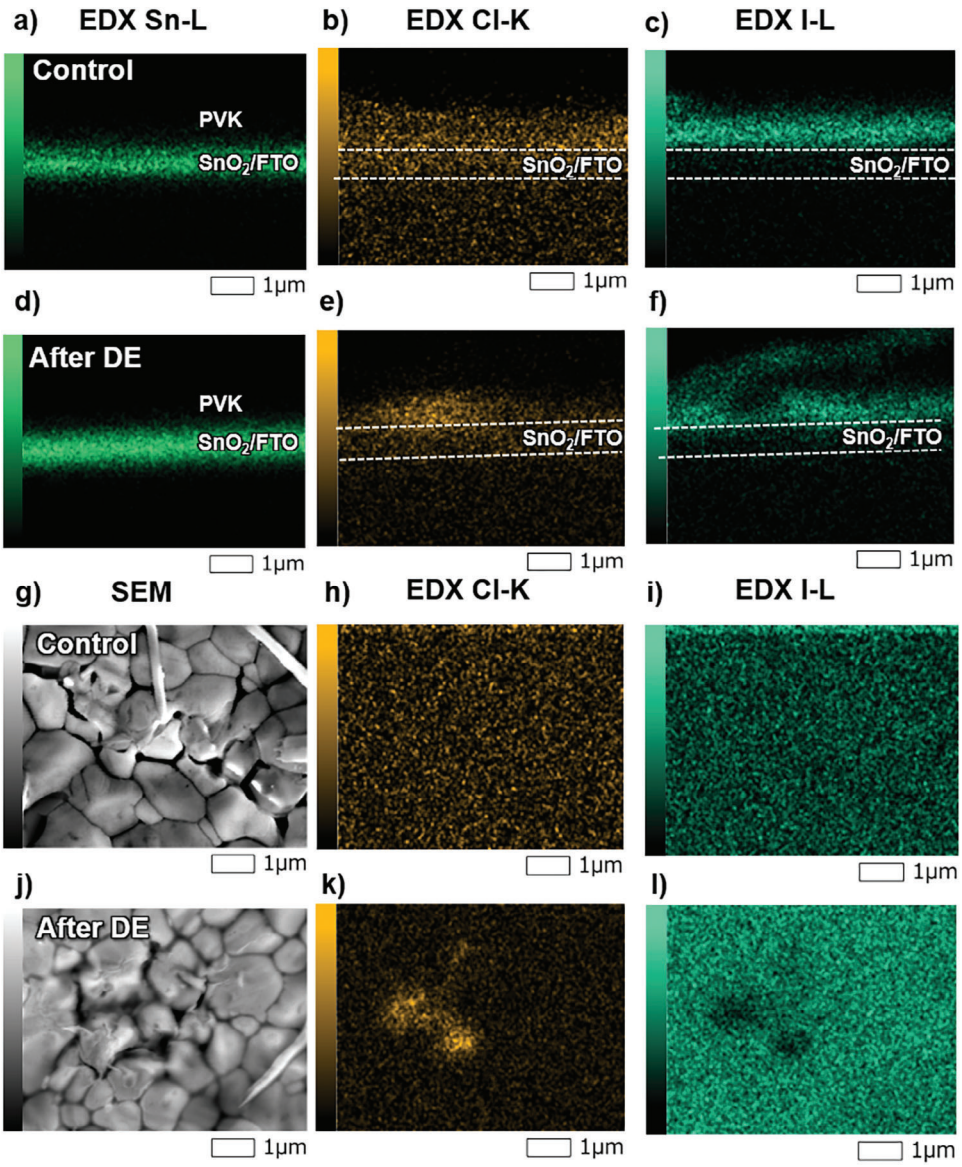

Figure 5. SEM-EDX maps (a–f, h–i, k–l) and SEM images (g, j) and of the MACl-added $FAPbI_3$ PSCs. Cross-sectional analyses of (a–c) control and (d–f) post-DE treatment samples. The white dashed lines in (b, c, e, f) represent a SnO_2/FTO layer from the EDX maps of Sn-L (a,d). Surface analyses of (g–i) control and (j–l) post-DE treatment samples.

irradiation, iodide anions migrate vertically away from the illuminated region[42] toward HTL in the present case. Similarly, during the positive biasing, iodide anions drift toward the HTL side. Thus, iodine species concentrate at the HTL/perovskite interface, leaving vacancies in the perovskite layer. The accumulation of these vacancies increases recombination, as indicated by the enhanced PL signal from the ETL side (Figure 3d). Eventually, the lack of carrier transport to the electrodes would lead to a cancellation of the photovoltaic effect. The remaining EQE signal in the 300–450 nm region may be tentatively explained by the presence of the δ-$FAPbI_3$ phase in the layer, as the EQE spectrum of a degraded **$FAPbI_3$ PSC 1** (Figure S6a, Supporting Information) looks like those of 3P, 7L, and DE. However, the EQE signal in the 450–800 nm region is still present, showing the presence of α-$FAPbI_3$. A photoabsorption spectrum of a completely degraded **$FAPbI_3$ PSC 2** is attributed to colorless δ-$FAPbI_3$ and is similar to the observed suppressed EQE spectra. An X-ray diffraction (XRD) pattern of **$FAPbI_3$ PSC 1** confirms the presence of only α and δ phases and the absence of photoactive PbI_2[43] (Figure S6b, Supporting Information). The mechanism of appearance and disappearance of δ-$FAPbI_3$-like response in EQE during DE and light soaking is still unknown, and its in-operando characterization is difficult. Thus, further investigations are needed.

To visualize ion migration directly, we performed SEM-EDX observations of samples with and without DE treatment. **Figure** 5a–c show Sn-L, Cl-K, and I-L EDX maps of a control sample, respectively, and demonstrate homogeneous distributions of

Cl^- and I^- in the perovskite layer (the SnO_2/FTO layer is identified from the Sn-L map). After DE treatment (Figure 5d–f), the Cl^- left from the residual MACl in the perovskite was redistributed, forming lumps on the surface and near the HTL (Figure 5e). A closer look revealed that the concentration of I^- at the Cl^- lump position was lower than that at other positions (Figure 5f), suggesting that I^- was displaced by Cl^- concentrating at defect sites. We also examined different samples and found that the complementary inhomogeneous redistributions of Cl^- and I^- were general phenomena (Figure S7, Supporting Information). Moreover, the distribution of Cl^- after DE treatment and subsequent light soaking is noteworthy. As shown in Figure S8 (Supporting Information), the Cl^- distribution largely reverted to a homogeneous shape after light soaking, although it was inhomogeneous immediately after DE treatment. We hypothesized that chlorine not only participates in ionic movements under an electric bias but also passivates defects at both interfaces. Furthermore, samples with MACl exhibited a Cl/I ratio twice as large as those without MACl (Figure S9, Supporting Information), proving the existence of residual Cl in our $FAPbI_3$.

To identify the locations of residual Cl^- lumps, we performed SEM-EDX on the top surface of the perovskite layer (Figure 5g–l). The Cl^- map after DE treatment shows lumps located at morphological imperfections, such as grain boundaries and pinholes. Another EDX map of different samples and locations after DE treatment (Figure S10, Supporting Information) also shows Cl^- condensation at pinholes. We confirmed that this Cl^- condensation is not due to Pb redistribution (the EDX peaks of Cl and Pb are relatively close: 2.62 and 2.34 eV, respectively), as evident from their different distribution maps (Figure S11, Supporting Information).

TOF-SIMS measurements further supported the vertical migration of Cl^- and I^- ions after DE treatment. As shown in **Figure 6**a, the intensity of Cl^- decreased throughout the bulk perovskite layer, while that of I^- decreased near the bottom SnO_2 ETL. Notably, the intensities of both Cl^- and I^- near the HTL/$FAPbI_3$ interface increased (Figure 6b), whereas that of PbI^- remained mostly constant. The concentration of Cl^- at the SnO_2/$FAPbI_3$ interface did not change significantly after DE treatment. This observed segregation of Cl^- at the ETL side is consistent with the reported TOF-SIMS profiles of MACl-added $FAPbI_3$.[29,44]

Based on these results, we propose a mechanism for Cl^- distribution after DE treatment and light soaking, as illustrated in **Figure 7**. Immediately after device preparation, the distribution of Cl^- is homogeneous both vertically and horizontally (Figure 7a). Under positive and negative biases (shaking bias) during DE treatment (Figure 7b), Cl^- drifts to the ETL and HTL sides, respectively, and concentrates at defect sites. The passivation role of Cl^- at the SnO_2/perovskite interface is well-documented in the literature.[45–48] However, Cl^- accumulation at the HTL side may block the holes and cause a temporary decrease in J_{SC} and EQE values. The light soaking promotes Cl^- migration and redistribution within the perovskite layer (Figure 7c). The migration of I^- is likely similar to that of Cl^-. Thus, applying DE treatment after PSC manufacturing ensures stable PSC function. This finding is particularly interesting in light of recent studies on the increased amount of MACl in the perovskite precursor and the role of residual Cl in this layer.[49]

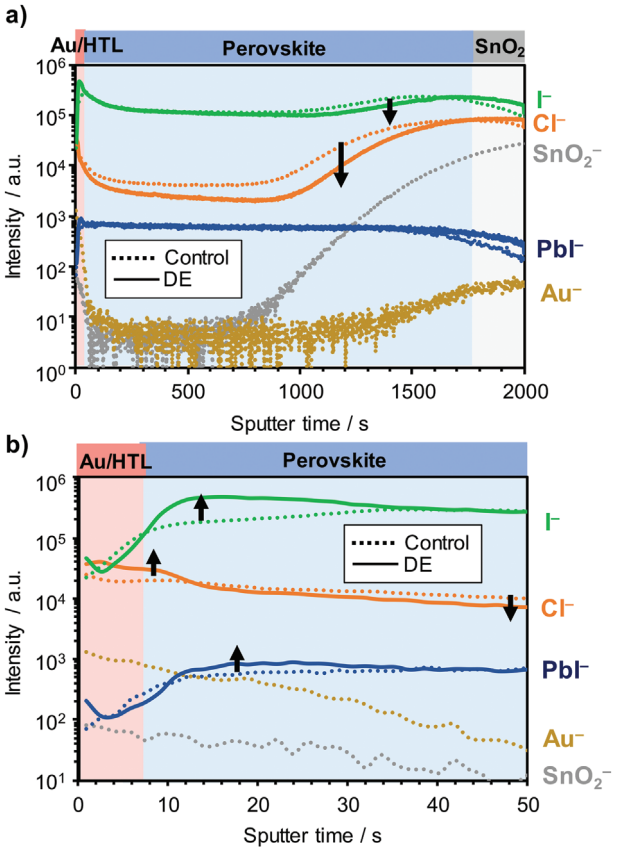

Figure 6. TOF-SIMS profiles of MACl-added $FAPbI_3$ devices after Ar sputtering for a) 0–2000 s and b) 0–40 s. The dotted and solid lines correspond to before (control) and after DE treatment (DE), respectively. The black arrows represent the change after DE treatment.

We also examined the DE treatment on MACl-free perovskite formulations, as shown in Figure S12 (Supporting Information). $FA_{0.80}MA_{0.15}Cs_{0.05}Pb(Br_{0.33}I_{0.67})_3$ (wide band gap) and $PEA_{0.1}FA_{0.9}SnI_3$ (tin, PEA: phenylethylammonium) perovskites showed significantly reduced PCE values (≈0%) after DE treatment. $MA_{0.13}FA_{0.87}Pb(I_{0.87}Br_{0.13})_3$ exhibited a decrease in overall PCE. These observations suggest that DE treatment is detrimental to these systems. However, DE treatment is highly effective for MACl-added $FAPbI_3$, simultaneously improving PCE and statistical deviation of device performance, understood through Cl^- defect passivation.

3. Conclusion

The DE treatment significantly improves the performance of MACl-added $FAPbI_3$ PSCs. This post-manufacturing treatment, combined with light soaking, facilitates the movement of halide anions to defect sites, resulting in an average PCE increase of 2.9 ± 1.8% (from an initial 18.2 ± 2.0% to 21.1 ± 0.8% after treatment). Notably, the improvement was more pronounced for initially low-performing devices than for high-performing ones, narrowing the deviation in device performance. SEM-EDX and

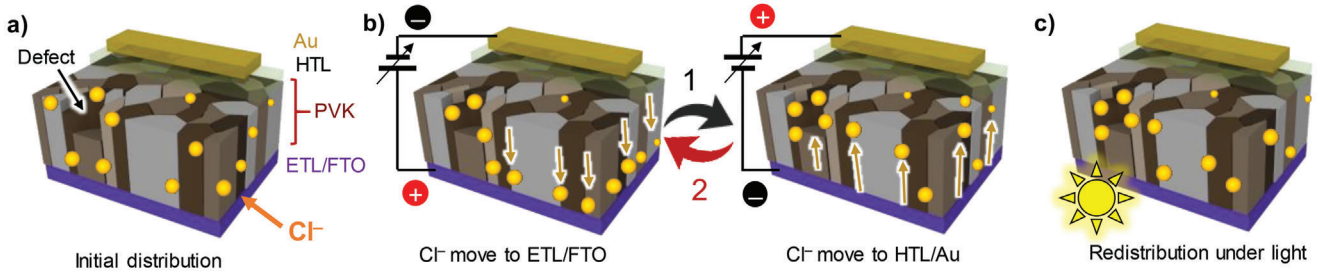

Figure 7. Schematic of Cl^- drift and migration by DE treatment and light soaking. a) Initial distribution, b) Cl^- movement during (left panel) negative and (right panel) positive biasing. c) Redistribution of Cl^- under light soaking. The reverse-forward biasing shown in (b) and light soaking during the *JV* measurement shown in (c) constitute one cycle of the DE treatment.

TOF-SIMS analyses of DE-treated cells revealed an increased concentration of Cl^- near the HTL/perovskite interface, particularly at morphological imperfections such as grain boundaries and pinholes. Therefore, DE treatment offers a promising approach for enhancing the efficiency and reproducibility of $FAPbI_3$-based PSCs, offering insights into the potential mechanisms underlying the observed improvements.

4. Experimental Section

Materials and PSC Fabrication: Fluorine-doped tin oxide (FTO) samples (8 Ω per sq, Sigma–Aldrich) were etched with HCl and Zn to create a pattern that prevents shunting. Next, a compact layer of SnO_2 was applied to the substrates by spin-coating an aqueous colloidal dispersion of SnO_2 (15 wt.% in H_2O, Thermo Fisher Scientific) that had been diluted with deionized water in a 1:3 volume ratio. Spin coating was performed at 3000 rpm for 30 s. The resulting films were then annealed on a hot plate at 120 °C for 30 min. Subsequently, the SnO_2 dispersion was further diluted to a 1:15 volume ratio and deposited using the same spin-coating process.[50] All the SnO_2 layers were passivated with lithium carbonate by spin-coating a 20 mM Li_2CO_3[51] (99%, Wako Chemical Corp., WAKO) aqueous solution at 3000 rpm for 30 s, followed by annealing at 100 °C for 15 min. The perovskite absorber layer was deposited in a nitrogen-filled glove box. The precursor solution for the perovskite was prepared by dissolving 455 mg (0.72 mmol) of $FAPbI_3$ powder and 14 mg (0.24 mmol) of methylammonium chloride (MACl; >99.99%, Greatcell Solar) in 400 µL of a solvent blend of *N*,*N*-dimethylformamide (DMF, super dehydrated, WAKO) and dimethyl sulfoxide (DMSO, super dehydrated, WAKO) at a volume ratio of 4:1 (1.8 M). Some samples were prepared using MACl-free precursors. The $FAPbI_3$ powder was synthesized according to a previously reported method.[52] To create the perovskite film, 65 µL of the precursor solution was spin-coated at 4000 rpm for 40 s. After spinning for 12 s, 200 µL of anhydrous ethyl acetate (99.8%, WAKO) was applied to the spinning sample from a distance of 5–6 cm. The sample was then annealed at 150 °C for 10 min in an environment with a temperature of 20–25 °C and 20–30% RH. Next, a 16 mM solution of benzamidine hydrochloride (>97.0%, Tokyo Chemical Inc., TCI) in a 1:1 volume mixture of anhydrous 2-propanol (>99.5%, WAKO) and anhydrous toluene (99.8%, WAKO) was spin-coated onto the perovskite film, followed by annealing at 100 °C for 5 min.[53] Next, 50 µL of the hole-transport layer (HTL) solution was prepared, containing 60 mM spiro-OMeTAD (>98.0%, TCI), 30 mM 4-tert-butylpyridine (TBP, 98%, Sigma–Aldrich), and 37 mM lithium bis(trifluoromethanesulfonyl)imide (>98.0%, TCI) dissolved in isopropanol (IPA). This solution was filtered using a syringe filter with a 0.22 µm pore size and then spin-coated onto the perovskite layers at 4500 rpm for 30 s. Finally, gold electrodes, ≈70 nm thick, were thermally evaporated onto the samples at an evaporation rate not exceeding 1 Å s^{-1}. The preparation of perovskite solar cells based on $MA_{0.13}FA_{0.87}Pb(I_{0.87}Br_{0.13})_3$, $FA_{0.80}MA_{0.15}Cs_{0.05}Pb(Br_{0.33}I_{0.67})_3$ and $PEA_{0.1}FA_{0.9}SnI_3$ can be found in the literature.[54–56] Additionally, samples for top-surface EDX were prepared by removing the gold electrode with scotch tape, and the HTL was removed using *o*-dichlorobenzene (>98.0%, WAKO). Hence, the perovskite layer was exposed for analysis.

Solar Cell Characterization and DE treatment: Current density-voltage curves were measured using a source meter unit (SMU) (ADCMT Corp., 6241A) under AM 1.5 G pseudo-solar illumination at 100 mW cm^{-2} using a 300 W solar simulator (SAN-EI, XES-301S, monitored by a calibrated standard cell of Bunko Keiki BS-520BK). The active area of the mask was 0.085 cm^2. The scan was conducted from 1.2 to 0 V and then backward, with a step size of 0.05 V and a hold time of 100 ms. The DE treatment with a voltage scan from −1.3 to 1.1 V, and back to −1.3 V, was performed with 0.02 V steps (holding time: 1 sec) using the same SMU. Following this treatment, V_{OC} was measured under 100 mW cm^{-2} illumination, showing a gradual increase until saturation. This process was repeated thrice on average to achieve the best performance. The EQE spectra were recorded using a Bunko Keiki SM-250KD equipped with a Keithley 2401 SMU. The monochromatic light power of the EQE instrument was calibrated using a silicon photovoltaic cell (Bunko Keiki model S1337-1010BQ). All the measurements were performed at 25 °C in the air.

General Measurements: Steady-state photoluminescence spectroscopy was performed using a Jasco FP-8300 spectrophotometer. Photoabsorption spectra were measured using Jasco V-730 spectrophotometer. SEM-EDX was performed on a field-emission SEM JEOL JSM-IT700HR instrument with an EDX JEOL JED-2300 at 5 and 10 keV. A small perturbation pump pulse at 532 nm was provided by a Nd:YAG laser (Spectra Physics Inc., GCR-100, 5–8 ns pulse duration, 10 Hz). The TPV generated by the laser pulse (1.0×10^{15} photons cm^{-2} $pulse^{-1}$) was monitored with a digital oscilloscope (Tektronix, DPO4104) with the input impedance of 1 MΩ to hold the device at open circuit. TOF-SIMS was performed using an M6 (IONTOF Corp.). The depth profile was obtained using an argon gas cluster ion beam at 5 keV for etching over an area of 200 × 200 µm with a target current of 3 nA. For the measurements, a primary ion beam of Bi^{3+} at 30 keV was utilized, conducted over an area of 100 × 100 µm with a target current of 0.4 pA.

Supporting Information

Supporting Information is available from the Wiley Online Library or from the author.

Acknowledgements

The authors acknowledge the financial support received from the New Energy and Industrial Technology Development Organization (NEDO) Green Innovation Project (JP21578854 to A.W. and A.S.), KAKENHI of the Japan Society for the Promotion of Science (JSPS) (JP20H05836 and JP24H00484 to A.S.), the Japan Science and Technology Agency (JST) CREST (JPMJCR23O2 to A.S.), MIRAI (JPMJMI22E2 to A.W. and A.S.), and PREST

(JPMJPR21A2 to I.F.), and International Collaborative Research Program of ICR, Kyoto University (Project No. 2024–43 to A.W. and A.S.). The authors thank Dr. Shaoxian Li and Ms. Tingting Liu at Osaka University for providing $MA_{0.13}FA_{0.87}Pb(I_{0.87}Br_{0.13})_3$ and $PEA_{0.1}FA_{0.9}SnI_3$ samples. The authors thank Dr. Shaoxian Li for his support with TPV measurements. The authors thank Ms. Nao Eguchi at SANKEN, Osaka University for the operation of TOF-SIMS measurements.

Conflict of Interest

The authors declare no conflict of interest.

Data Availability Statement

The data that support the findings of this study are available in the supplementary material of this article.

Keywords

dark electro treatment, formamidinium lead iodide perovskite, light soaking, methylammonium chloride, passivation

Received: July 18, 2024
Revised: August 23, 2024
Published online:

[1] Y. Zhao, F. Ma, Z. Qu, S. Yu, T. Shen, H. X. Deng, X. Chu, X. Peng, Y. Yuan, X. Zhang, J. You, *Science* **2022**, *377*, 531.
[2] R. Azmi, D. S. Utomo, B. Vishal, S. Zhumagali, P. Dally, A. M. Risqi, A. Prasetio, E. Ugur, F. Cao, I. F. Imran, A. A. Said, A. R. Pininti, A. S. Subbiah, E. Aydin, C. Xiao, S. Il Seok, S. De Wolf, *Nature* **2024**, *628*, 93.
[3] J. Park, J. Kim, H. S. Yun, M. J. Paik, E. Noh, H. J. Mun, M. G. Kim, T. J. Shin, S. Il. Seok, *Nature* **2023**, *616*, 724.
[4] Z. Liang, Y. Zhang, H. Xu, W. Chen, B. Liu, J. Zhang, H. Zhang, Z. Wang, D. H. Kang, J. Zeng, X. Gao, Q. Wang, H. Hu, H. Zhou, X. Cai, X. Tian, P. Reiss, B. Xu, T. Kirchartz, Z. Xiao, S. Dai, N. G. Park, J. Ye, X. Pan, *Nature* **2023**, *624*, 557.
[5] S. Ghosh, S. K. Pal, K. J. Karki, T. Pullerits, *ACS Energy Lett.* **2017**, *2*, 2133.
[6] C. Wang, D. Qu, B. Zhou, C. Shang, X. Zhang, Y. Tu, W. Huang, *Small* **2024**, *20*, 2307645.
[7] K. Domanski, B. Roose, T. Matsui, M. Saliba, S. H. Turren-Cruz, J. P. Correa-Baena, C. R. Carmona, G. Richardson, J. M. Foster, F. De Angelis, J. M. Ball, A. Petrozza, N. Mine, M. K. Nazeeruddin, W. Tress, M. Grätzel, U. Steiner, A. Hagfeldt, A. Abate, *Energy Environ. Sci.* **2017**, *10*, 604.
[8] D. J. Slotcavage, H. I. Karunadasa, M. D. McGehee, *ACS Energy Lett.* **2016**, *1*, 1199.
[9] D. Klotz, G. Tumen-Ulzii, C. Qin, T. Matsushima, C. Adachi, *RSC Adv.* **2019**, *9*, 33436.
[10] R. Su, Z. Xu, J. Wu, D. Luo, Q. Hu, W. Yang, X. Yang, R. Zhang, H. Yu, T. P. Russell, Q. Gong, W. Zhang, R. Zhu, *Nat. Commun.* **2021**, *12*, 2479.
[11] H. Elbohy, H. Suzuki, T. Nishikawa, A. K. K. Kyaw, Y. Hayashi, *ACS Appl. Energy Mater.* **2024**, *7*, 2925.
[12] U. Das, P. K. Sarkar, S. K. Sharma, R. Deb, R. Garg, B. Prakash, K. Parida, A. Roy, *J. Phys. Chem. C* **2024**, *128*, 3043.
[13] Y. Wang, J. Chen, Y. Zhang, W. L. Tan, Z. Ku, Y. Yuan, Q. Chen, W. Huang, C. R. McNeill, Y. Cheng, J. Lu, *Adv. Mater.* **2024**, *36*, 2401416.
[14] P. Chen, Y. Xiao, J. Hu, S. Li, D. Luo, R. Su, P. Caprioglio, P. Kaienburg, X. Jia, N. Chen, J. Wu, Y. Sui, P. Tang, H. Yan, T. Huang, M. Yu, Q. Li, L. Zhao, C. H. Hou, Y. W. You, J. J. Shyue, D. Wang, X. Li, Q. Zhao, Q. Gong, Z. H. Lu, H. J. Snaith, R. Zhu, *Nature* **2024**, *625*, 516.
[15] W. Tress, N. Marinova, T. Moehl, S. M. Zakeeruddin, M. K. Nazeeruddin, M. Grätzel, *Energy Environ. Sci.* **2015**, *8*, 995.
[16] D. Moia, I. Gelmetti, P. Calado, W. Fisher, M. Stringer, O. Game, Y. Hu, P. Docampo, D. Lidzey, E. Palomares, J. Nelson, P. R. F. Barnes, *Energy Environ. Sci.* **2019**, *12*, 1296.
[17] O. Hentz, P. Rekemeyer, S. Gradečak, *Adv. Energy Mater.* **2018**, *8*, 1701378.
[18] L. Lin, L. Yang, G. Du, X. Li, Y.-n. Li, J. Deng, K. Wei, J. Zhang, *ACS Appl. Energy Mater.* **2023**, *6*, 10303.
[19] K. Huang, X. Feng, H. Li, C. Long, B. Liu, J. Shi, Q. Meng, K. Weber, T. Duong, J. Yang, *Adv. Sci.* **2022**, *9*, 2204163.
[20] K. Jeong, J. Byeon, J. Jang, N. Ahn, M. Choi, *Joule* **2022**, *6*, 1087.
[21] H. T. Pham, Y. Yin, G. Andersson, K. J. Weber, T. Duong, J. Wong-Leung, *Nano Energy* **2021**, *87*, 106226.
[22] M. Jeong, I. W. Choi, E. M. Go, Y. Cho, M. Kim, B. Lee, S. Jeong, Y. Jo, H. W. Choi, J. Lee, J. H. Bae, S. K. Kwak, D. S. Kim, C. Yang, *Science* **2020**, *369*, 1615.
[23] M. Kim, T. K. Lee, I. W. Choi, H. W. Choi, Y. Jo, J. Lee, G. H. Kim, S. K. Kwak, D. S. Kim, *Sustain. Energy Fuels* **2020**, *4*, 3753.
[24] K. O. Kosmatos, L. Theofylaktos, E. Giannakaki, D. Deligiannis, M. Konstantakou, T. Stergiopoulos, *Energy Environ. Mater.* **2019**, *2*, 79.
[25] J. Bing, D. S. Lee, Y. Cho, J. Zheng, Y. Li, S. Tang, M. Zhang, S. Huang, A. W. Y. Ho-Baillie, *Mater. Today Energy* **2020**, *18*, 100551.
[26] Y. Zhao, K. Zhu, *J. Am. Chem. Soc.* **2014**, *136*, 12241.
[27] J. Hu, J. W. Ahn, Z. Xu, M. J. Jeong, C. Kim, J. H. Noh, H. Min, B. P. Rand, *Adv. Energy Mater.* **2024**, *14*, 2400500.
[28] S. Takahashi, S. Uchida, H. Segawa, *ACS Omega* **2023**, *8*, 42711.
[29] L. Yuan, J. Wang, P. Huang, Q. Yin, S. Zou, L. Wang, Z. Zhang, H. Luo, F. Liu, J. Qiu, J. Xie, L. Ding, K. Yan, *Small Methods* **2023**, *7*, 2201467.
[30] N. Rybin, D. Ghosh, J. Tisdale, S. Shrestha, M. Yoho, D. Vo, J. Even, C. Katan, W. Nie, A. J. Neukirch, S. Tretiak, *Chem. Mater.* **2020**, *32*, 1854.
[31] C. Eames, J. M. Frost, P. R. F. Barnes, B. C. O'Regan, A. Walsh, M. S. Islam, *Nat. Commun.* **2015**, *6*, 7497.
[32] C. Ruan, L. He, L. Zhu, B. Yuan, H. Yang, G. Qin, Y. Chen, Q. Tao, *J. Alloys Compd.* **2024**, *999*, 174990.
[33] H. Zhang, L. Pfeifer, S. M. Zakeeruddin, J. Chu, M. Grätzel, *Nat. Rev. Chem.* **2023**, *7*, 632.
[34] C. Zhao, H. Zhang, M. Almalki, J. Xu, A. Krishna, F. T. Eickemeyer, J. Gao, Y. M. Wu, S. M. Zakeeruddin, J. Chu, J. Yao, M. Grätzel, *Adv. Mater.* **2023**, *35*, 2211619.
[35] J. M. Frost, A. Walsh, *Acc. Chem. Res.* **2016**, *49*, 528.
[36] B. Chen, P. N. Rudd, S. Yang, Y. Yuan, J. Huang, *Chem. Soc. Rev.* **2019**, *48*, 3842.
[37] J. Herterich, M. Unmüssig, G. Loukeris, M. Kohlstädt, U. Würfel, *Energy Technol.* **2021**, *9*, 2001104.
[38] W. Nie, J. C. Blancon, A. J. Neukirch, K. Appavoo, H. Tsai, M. Chhowalla, M. A. Alam, M. Y. Sfeir, C. Katan, J. Even, S. Tretiak, J. J. Crochet, G. Gupta, A. D. Mohite, *Nat. Commun.* **2016**, *7*, 11574.
[39] Y. Cho, H. Do Kim, J. Zheng, J. Bing, Y. Li, M. Zhang, M. A. Green, A. Wakamiya, S. Huang, H. Ohkita, A. W. Y. Ho-Baillie, *ACS Energy Lett.* **2021**, *6*, 925.
[40] J. Zhuang, J. Wang, F. Yan, *Nano-Micro Lett.* **2023**, *15*, 84.
[41] J. Thiesbrummel, V. M. Le Corre, F. Peña-Camargo, L. Perdigón-Toro, F. Lang, F. Yang, M. Grischek, E. Gutierrez-Partida, J. Warby, M. D. Farrar, S. Mahesh, P. Caprioglio, S. Albrecht, D. Neher, H. J. Snaith, M. Stolterfoht, *Adv. Energy Mater.* **2021**, *11*, 2101447.
[42] D. W. de Quilettes, W. Zhang, V. M. Burlakov, D. J. Graham, T. Leijtens, A. Osherov, V. Bulović, H. J. Snaith, D. S. Ginger, S. D. Stranks, *Nat. Commun.* **2016**, *7*, 11683.

[43] J. B. Patel, Q. Lin, O. Zadvorna, C. L. Davies, L. M. Herz, M. B. Johnston, *J. Phys. Chem. Lett.* **2018**, *9*, 263.
[44] V. Larini, M. Degani, G. Pica, C. Ding, Z. Andaji-Garmaroudi, F. Faini, S. D. Stranks, C. Q. Ma, G. Grancini, *Sol. RRL* **2022**, *6*, 2200038.
[45] C. Zhao, Q. Zhang, Y. Lyu, X. Lian, K. Wang, F. Shen, M. Luo, H. Liu, H. Han, F. Xie, X. Mo, Y. Yang, J. Xu, A. K.-Y. Jen, H. Zhang, J. Yao, *ACS Energy Lett.* **2024**, *9*, 1405.
[46] M. Hatamvand, S. Gholipour, M. Chen, Y. Zhou, T. Jiang, Z. Hu, Y. Chen, W. Huang, *Chem. Eng. J.* **2023**, *460*, 141788.
[47] S. Kim, F. Zhang, J. Tong, X. Chen, E. Enkhbayar, K. Zhu, J. Kim, *Sol. Energy* **2022**, *233*, 353.
[48] Z. Li, C. Kolodziej, C. McCleese, L. Wang, A. Kovalsky, A. C. Samia, Y. Zhao, C. Burda, *Nanoscale Adv* **2019**, *1*, 827.
[49] D. H. Kang, S. U. Lee, N. G. Park, *ACS Energy Lett.* **2023**, *8*, 2122.
[50] M. Pylnev, R. Nishikubo, F. Ishiwari, A. Wakamiya, A. Saeki, *Sol. RRL* **2024**, *8*, 2400415.
[51] Y. Zhang, T. Kong, H. Xie, J. Song, Y. Li, Y. Ai, Y. Han, D. Bi, *ACS Energy Lett.* **2022**, *7*, 929.
[52] Y. Zhang, S. Seo, S. Y. Lim, Y. Kim, S. G. Kim, D. K. Lee, S. H. Lee, H. Shin, H. Cheong, N. G. Park, *ACS Energy Lett.* **2020**, *5*, 360.
[53] F. Ye, T. Tian, J. Su, R. Jiang, J. Li, C. Jin, J. Tong, S. Bai, F. Huang, P. Müller-Buschbaum, Y. Cheng, T. Bu, *Adv. Energy Mater.* **2024**, *14*, 2302775.
[54] N. Minoi, F. Ishiwari, K. Murotani, R. Nishikubo, T. Fukushima, A. Saeki, *ACS Appl. Mater. Interfaces* **2023**, *15*, 6708.
[55] Y. Park, R. Nishikubo, A. Saeki, *J. Photopolym. Sci. Technol.* **2023**, *36*, 359.
[56] Y. Miyamoto, S. Kusumoto, T. Yokoyama, Y. Nishitani, T. Matsui, T. Kouzaki, R. Nishikubo, A. Saeki, Y. Kaneko, *ACS Appl. Nano Mater* **2020**, *3*, 11650.